Video Article

Modeling and Simulations of Olfactory Drug Delivery with Passive and Active Controls of Nasally Inhaled Pharmaceutical Aerosols

Xiuhua A. Si[1], Jinxiang Xi[2]

[1]Department of Mechanical Engineering, California Baptist University

[2]School of Engineering and Technology, Central Michigan University

Correspondence to: Xiuhua A. Si at asi@calbaptist.edu

URL: https://www.jove.com/video/53902
DOI: doi:10.3791/53902

Keywords: Medicine, Issue 111, Direct nose-to-brain delivery, neurological medication, olfactory deposition, active particle control, magnetophoretic guidance

Date Published: 5/20/2016

Citation: Si, X.A., Xi, J. Modeling and Simulations of Olfactory Drug Delivery with Passive and Active Controls of Nasally Inhaled Pharmaceutical Aerosols. *J. Vis. Exp.* (111), e53902, doi:10.3791/53902 (2016).

Abstract

There are many advantages of direct nose-to-brain drug delivery in the treatment of neurological disorders. However, its application is limited by the extremely low delivery efficiency (< 1%) to the olfactory mucosa that directly connects the brain. It is crucial to develop novel techniques to deliver neurological medications more effectively to the olfactory region. The objective of this study is to develop a numerical platform to simulate and improve intranasal olfactory drug delivery. A coupled image-CFD method was presented that synthetized the image-based model development, quality meshing, fluid simulation, and magnetic particle tracking. With this method, performances of three intranasal delivery protocols were numerically assessed and compared. Influences of breathing maneuvers, magnet layout, magnetic field strength, drug release position, and particle size on the olfactory dosage were also numerically studied.

From the simulations, we found that clinically significant olfactory dosage (up to 45%) were feasible using the combination of magnet layout and selective drug release. A 64 -fold higher delivery of dosage was predicted in the case with magnetophoretic guidance compared to the case without it. However, precise guidance of nasally inhaled aerosols to the olfactory region remains challenging due to the unstable nature of magnetophoresis, as well as the high sensitivity of olfactory dosage to patient-, device-, and particle-related factors.

Video Link

The video component of this article can be found at https://www.jove.com/video/53902/

Introduction

Drugs delivered to the olfactory region can bypass the blood-brain-barrier and directly enter the brain, leading to an efficient uptake and quick action onset of the drugs[1,2]. However, conventional nasal devices such as nasal pumps and sprays deliver extremely low doses to the olfactory region (< 1%) via the nasal route[3,4]. It is primarily due to the complicated structure of the human nose which is composed of narrow, convoluted passageways (**Figure 1**). The olfactory region locates above the superior meatus, where only a very small fraction of inhaled air can reach[5,6]. Furthermore, conventional inhalation devices depend on aerodynamic forces to transport therapeutic agents to the target area[7]. There is no further control over the motions of particles after their release. Therefore, the transport and deposition of these particles predominately depend on their initial speeds and release positions. Due to the convoluted nasal passage as well as the lack of particle control, the majority of drug particles are trapped in the anterior nose and cannot reach the olfactory region[8].

While there are many choices of nasal devices, those designed specifically for targeted olfactory delivery have rarely been reported[7,9]. One exception is Hoekman and Ho[10] who developed an olfactory-preferential delivery device and demonstrated higher cortex-to-blood drug levels in rats as opposed to using a nose drop. However, scaling the deposition results in rats to humans is not straightforward, considering the vast anatomical and physiological differences between these two species[11]. Many limitations exist when using adapted versions of standard nasal devices for olfactory deliveries. One primary setback is that only a very small portion of medications can be delivered to the olfactory mucosa, through which the medications may enter the brain. Numerical modeling predicted that less than 0.5% of intranasally administered nanoparticles can deposit in the olfactory region[3,5]. The deposition rate is even lower (0.007%) for micrometer particles[12]. In order to make the nose-to-brain delivery clinically feasible, the olfactory deposition rate has to be significantly improved.

There exist several possible approaches to improve the olfactory delivery. One approach is the smart inhaler idea proposed by Kleinstreuer *et al.*[13] As particles depositing in one region are mainly from one specific area at the inlet, it is possible to deliver particles to the target site by releasing them only from certain areas at the inlet. The smart delivery technique has been shown to generate a much more efficient lung delivery than conventional methods.[13,14] It is hypothesized that this *smart* delivery idea can also be applied in intranasal drug delivery to improve dosages to the olfactory mucosa. By releasing particles into different positions at the nostril opening and from different depths within the nasal cavity, improved olfactory delivery efficiencies and reduced drug waste in the anterior nose are possible.

Another possible method is to actively control the particle motion within the nasal cavity using a variety of field forces, such as electric or magnetic force. Electric control of charged particles has been suggested for targeted drug delivery to the human nose and lungs[15-17]. Xi *et al.*[18] numerically tested the performance of electric guidance of charged particles and predicted significantly improved olfactory doses. Similarly, guidance of ferromagnetic drug particles with an appropriate magnetic field also has the potential to target particles to the olfactory mucosa. Behaviors of inhaled agents, if ferromagnetic, can be altered by imposing appropriate magnetic forces[19]. Dames *et al.*[20] demonstrated that it is practical to target ferromagnetic particles to specific areas in mouse lungs. By packaging therapeutic agents with superparamagnetic iron oxide nanoparticles, the deposition in one lung of a mouse under the influence of a strong magnetic field was significantly increased compared to the other lung[20].

Particles were assumed to be spherical and ranged from 150 nm to 30 μm in diameter. The governing equation is[21]:

$$(1)\quad \frac{d\left(m_p v_i\right)}{dt} = \frac{f}{\tau_p C_c} m_p\left(u_i - v_i\right) + m_p g_i\left(1-\alpha\right) + F_{i,Lift} + F_{Brownian} + F_{i,Magnetophoretic}$$

The above equation describes the motion of a particle governed by drag force, gravitational force, Saffman lift force [22], Brownian force for nanoparticles, and magnetophoretic force if placed in a magnetic field. Here, v_i is the particle velocity, u_i is the flow velocity, τ_p is the particle response time, C_c is the Cunningham correction factor, and α is the air/particle density ratio. To effectively guide the intranasally administered drugs to the olfactory region, it is necessary for the applied magnetophoretic forces to overcome both the particle inertia and gravitational force. In this study, a composite of 20% maghemite (γ-Fe_2O_3, 4.9 g/cm^3) and 80% active agent was assumed, which give a density of approximate 1.78 g/cm^3 and a relative permeability of 50. The selection of γ-Fe_2O_3 was due to its low cytotoxic. Iron (3+) ions are widely found in human body and a slightly higher ion concentration will not cause significant side-effects[23].

Protocol

The MRI images were provided by the Hamner Institutes for Health Sciences and the usage of these images was approved by the Virginia Commonwealth University institutional review board.

1. Image-Based Nasal Airway Preparation

1. Acquire magnetic resonance (MR) images of a healthy non-smoking 53-year-old male (weight 73 kg and height 173 cm) that consist of 72 coronal cross-sections spaced 1.5 mm apart spanning the nostrils to the nasopharynx[4].
2. **Open Imaging Program (*e.g.*, MIMICS)**
    1. To import images, click "File", "Import images". Select the MR images and click "Ok".
    2. To construct the 3-D model, click "Segmentation", then "Threshold" to set the grey scale range between -1020 and -500. Click "Segmentation", "Calculate 3D".
    3. Click "Segmentation" and "Calculate polylines". Select the 3-D body, and click "Ok" to generate the polylines that define the solid geometry. Export the polylines as an IGES file.
3. **Open Model Development Software (*e.g.*, Gambit)**
    1. Click "File", "Import", "IGES" to import the IGES file into the program. Click "Edge command button" on the right panel; click "Create Edge" and select "NURBS" to reconstruct smooth contours.
    2. Click "Face command button", then click "Form face". Select "Wireframe" to build a surface from edges. Continue to build all surfaces that cover the whole airway. Retain the nasal anatomical details such as the uvula, epiglottal fold, and laryngeal sinus (**Figure 1**). Click "File", "Export" "IGES" to export the nasal airway model.
4. **Open Meshing Software (*e.g.*, ICEM CFD)**
    1. Click "File", "Import Geometry", "Legacy" and "STEP/IES" to import the nasal airway model. Click "Create Parts" to divide the airway surfaces into five different regions: nasal vestibule, nasal valve, turbinate region, olfactory, and nasopharynx.
    2. To generate computational mesh inside the airway, click "Mesh", "Global Mesh Setup". Specify the maximum mesh size as 0.1 mm and click "Apply".
    3. To add a body-fitted mesh in the near-wall region, click "Compute Mesh", "Prism Mesh". Specify the number of layers as 5 and the expanding ratio as 1.25 and click "Apply".

2. Passive Control of Particles

1. **Vestibular Intubation: Front *vs.* Back**
    1. Open Model Development Software to develop the nasal model with front vestibular intubation. Click "Volume", then "Move/copy" to change the location of the nebulizer catheter 5 mm into the vestibule from nostril tip. Click "injection" to release 60,000 particles (150 nm) into the nostril.
    2. Open the fluid simulation software (*e.g.*, ANSYS Fluent) to compute particle deposition rates inside the nose. To compute the airflow field inside the airway, select the laminar flow model by clicking "Define", "Models", "Viscous"; chose "Laminar" under "Viscous model".
    3. Select the "Discrete Phase Model" to track particle motions. Check "Saffman Lift Force" under "Discrete Phase Model". Click "Report", then choose "Sample Trajectories"; select "nasal" under "Boundaries" and click "Compute" to find the number of particles deposited in the predefined olfactory region. Calculate the deposition rate as the ratio of the amount of deposited particles to the amount of particles entering the nostrils.
    4. Repeat steps 2.1.2 for 1 μm particles.

5. Follow the step 2.1.1, insert the spray nozzle 5 mm into the vestibule from the back of the nostril. Repeat steps 2.1.2, and 2.1.3 to compute deposition rate for 150 nm particles. Repeat step 2.1.4 for 1 µm particles (back-intubation).

2. **Deep Intubation**
   1. Follow procedure 2.1.1 to insert the nebulizer catheter right beneath the olfactory region. Release 60,000 submicron particles (150 nm) from the nebulizer.
   2. Use fluid and simulation software to compute particle deposition rates inside the nose on both total and local basis by following similar procedures as listed in 2.1.2. Repeat this procedure for 1 µm particles.
   3. Repeat the above procedures while exercising breathing-holding and exhalation, respectively. Click "Define", then "Boundary Conditions" to open the boundary condition panel. Specify zero velocity at the two nostrils for breathing-holding. Specify vacuum pressure (200 Pa) at the nostrils and zero pressure at the outlet for exhalation.

3. Active Control: Magnetophoretic Guidance

1. **Test in a Two-Plate Channel**
   1. Open magnetic particle tracking software (*e.g.*, COMSOL). Click "Geometry", and "Rectangle" to build the two-plate channel. Click "Rectangle" to build the magnets around the two-plate channel.
   2. Compute the particle trajectories and deposition rate. Click "Model 1", "Laminar flow" and "Inlet 1"; specify the inlet velocity as 0.5 m/s. Click "Model 1", "Magnetic Fields", and "Magnetic Flux Conservation", specify the strength of the three magnets (1×10^5 A/m).
   3. Click "Model 1", "Particle Tracking for Fluid Flow", and "Particle Properties"; specify the particle diameter (15 µm), density (1.78 g/cm^3). Click "Inlet" to release 3,000 particles. Click "Magnetophoretic Force", specify particle relative permeability (50). Click "Compute".
   4. To find how many particles depositing in the selected area, click "Results", "1D Plot Group" and "Plot". Calculate the deposition rate as the ratio of the amount of particle deposited in certain area to the amount of particles entering the geometry.
   5. To adjust the magnet strength, click "Model 1", then "Magnetic Fields"; choose "Magnetic Flux Conservation", and change the magnet strength under "Magnetization". Increase the magnet strength by an increment of 1×10^4 A/m and click "Compute".
   6. Repeat this procedure until the appropriate magnets arrangement was obtained for effective drug delivery to the olfactory region.

2. **Test in the 2-D Idealized Nose Model**
   1. Apply the magnetic strengths obtained in 3.1 into a 2-D nose model by putting three magnets 1 mm above the nose. Click "Model 1", "Geometry 1" to specify the size and position of the magnet. Click "Model 1", "Particle Tracking for Fluid Flow", "Inlet" to release 3,000 particles into the left nostril. Click "Particle Properties" to specify the particle size as 15 µm.
   2. Simulate the particle trajectories and subsequent olfactory delivery efficiencies by following similar procedures as listed in 3.1.2.
   3. Adjust the magnet layout and strength to improve olfactory delivery efficiency. To adjust the magnet size and position, click "Model 1", then "Geometry 1"; choose the magnet of interest, change the values of width, depth, height or *x, y, z*. Follow 3.1.5 to adjust the magnet strength.

3. **Test in the 3-D Anatomically Accurate Nose Model**
   1. Import the 3-D nasal airway model into Magnetic Particle Tracking software. Follow the procedure 3.2.1, put four magnets 1 mm above the nose and release 3,000 particles of 15 µm in diameter from one selected point only.
   2. Use Magnetic Particle Tracking software to track particle trajectories and compute olfactory delivery efficiencies by following similar procedures as listed in 3.2.1 - 3.2.3.
   3. Following 3.2.3, adjust the magnet layout and strength in the 3D model to improve the targeted delivery to the olfactory region.
   4. Test particle size ranging from 1 - 30 µm to find the right particle size for optimal magnetophoretic guidance to the olfactory region.

Representative Results

Control Case:
Figure 3 displays the airflow field and particle deposition in the nasal airway with standard nasal devices. It clearly shows that airflow from the front nostril is ventilated to the upper passage and airflow from the back nostril is directed towards the nasal floor (**Figure 3A**). Aerosol particles are observed to move faster in the median passages and slower near the walls, forming an aerosol front in the mean flow direction. Aerosol particles can reach the olfactory region in 0.02 to 0.03 sec after entering the nostril under normal breathing conditions (20 L/min) (**Figure 3B**). Very few particles (0.22%) deposit in the upper nose (superior meatus); even fewer particles (0.007%) reach the uppermost olfactory mucosa (**Figure 3C**). Highly heterogeneous deposition patterns were predicted, as illustrated by the wide range of deposition enhancement factor (DEF) in **Figure 3C**. Here, the DEF denotes the level of local particle accumulation and is computed as the ratio of local deposition rate over regional-averaged deposition rate in the nose[24]. The numerical model in this study was also validated against experimental data obtained in a comparable nasal airway replica. Good agreement was achieved between the numerically predicted and experimental measurements (**Figure 3D**).

Passive Control I: Vestibular Intubation

The simulation results of the vestibular intubation protocol are shown in **Figure 4**. For both the front and back intubation cases, there is a strong jet effect immediately downstream of the nozzle (**Figure 4A**). It is expected that particles released into the front vestibule will more likely deposit in the olfactory region than in other regions. Considering the back intubation case, the main flow is sucked downwards by the vacuum induced by the jet effect (**Figure 4B**). As expected, more drug particles are delivered to the olfactory region with the front intubation protocol in comparison to the back protocol. In addition, more focused deposition is observed in the olfactory region with the front release. The maximum DEF value is around 2.5 times that of the back release.

From **Figure 4C**, the difference of deposition rates is insignificant among the three cases (control, front, back). However, a dramatic difference exists in the olfactory deposition with the front-release giving significantly higher olfactory dosage, approximately twice that of the back-release case and ten times that of the control case.

Passive Control II: Deep Intubation with Different Breathing Maneuvers

In this protocol, the spray nozzle was inserted close to the olfactory mucosa. This positioning successfully bypassed the nasal valve, the major flow-limiting area in the nose. Three breathing conditions (inhalation, breath-holding, and exhalation) were considered regarding their influences on the olfactory drug delivery. Normal breathing rate (20 L/min) was used in both inhalation and exhalation conditions. Among the three breathing conditions, inhalation gave the highest dose as displayed by the concentrated olfactory depositions (**Figure 5A**). In contrast, both breath-holding and exhalation conditions failed to generate focused depositions. Clues to the diffusive deposition pattern can be obtained in nasal aerodynamics shown in **Figures 5B & c**, where only a small portion of the airflow goes to the olfactory region while the majority moves downwards either to the lung (**Figure 5B**) or exits to the ambient air (**Figure 5C**). In particular, particles in the exhalation case are dispersed throughout the nasal passages with no apparent deposition hot spots. Instead, for the inhalation case, high DEF values are restricted to the olfactory region only, with low DEF values observed in the turbinate region. This is an ideal deposition pattern, as it will maximize the therapeutic outcome in the targeted olfactory region while minimizing side effects in other regions.

The performance between the two delivery methods (vestibular *vs.* deep intubations) was further compared as a function of deposition rate per unit area (%/cm^2) in **Figure 5D**. The surface area of the olfactory region was 6.8 cm^2 in this study. Higher olfactory dosage per unit area was delivered with the deep intubation in comparison to the vestibular intubation. Specifically, the deep intubation under inhalation conditions delivered 2.5 times higher dose than that of the front vestibule release recommended in the first protocol. It should be noted that the deposited dosage still needs to diffuse across the olfactory epithelium before entering the cerebrospinal fluids.

Active Control: Magnetophoretic Guidance

Three geometries were employed in the numerical experiments of active particle controls: a two-plate channel to find the working magnet strength, an idealized 2-D nose model to find a baseline magnet layout, and an image-based 3-D nose model to test the performance and refine operating parameters of the magnetophoretic guidance protocol. **Figure 6A** shows the simulation results of two trials in the two-plate channel. In the first trial, we tested the feasibility of controlling particle motions by using magnetophoretic forces to counteract gravity, allowing the particles to move horizontally instead of falling. To this purpose, we applied three magnets on top of the channel (upper panel of **Figure 6A**). The resultant magnet field was stronger at the upper plate and weaker at the bottom plate. The ferromagnetic particles were attracted upward to the stronger magnetic field, which acted against gravity. When all three magnets had a volume magnetization of 1×10^5 A/m and the given particle size was 15 μm, the magnetophoretic force was in equilibrium with the gravitational force at the centerline of the channel (upper panel of **Figure 6A**).

The second trial tested how the particle trajectories changed when stronger magnets were applied (lower panel of **Figure 6A**). In this trial, the left two magnets were kept at 1×10^5 A/m, while the right magnet was increased to 1×10^6 A/m. Since the magnetic field was much stronger on the right side, all particles that passed through the left half of the channel turned their direction upward and deposited in the proximity of the third magnet. This trial demonstrated that when the magnetophoretic force was strong enough, the particle motion could be manipulated to reach the target site.

The performance of the magnetophoretic guidance was further assessed in an idealized 2-D nose model. One row of magnets was applied on the top of the nasal airway to attract the ferromagnetic particles upwards to the olfactory region. **Figure 4C** shows the particle transport and deposition after releasing the particles from one point at the tip of the nostril with a different magnet layout. It is shown that particle trajectories deviate upward due to the presence of magnets above the nose (**Figure 6B**). Furthermore, with appropriate magnet strength (1×10^6 A/m in Case 3), the majority of magnetophoretic-driven particles from this point deposits in the olfactory region (~ 92%). By contrast, an inadequate magnet field yields less pronounced magnetic responsiveness (Cases 1&2). In the absence of magnets, nearly no particles deposit onto the olfactory region even though the particles will pass by the olfactory region (**Figure 6B**).

Simulation results in the 3-D nose model under magnetophoretic guidance are shown in **Figure 7**. Following the parameters obtained in the 2-D nose model, magnets with a volume magnetization 1×10^6 A/m were initially employed. However, the olfactory delivery in this initial trial did not show promising results, presumably due to inadequate upward magnetophoretic force to reverse the particle motion. To identify the appropriate magnet strength for effective olfactory deliveries, a variety of volume magnetizations were tested by progressively increasing from 1×10^6 A/m by an increment of 1×10^5 A/m. It was observed that by increasing the maximum magnetization to 7.1×10^7 A/m, about 33% of the administered particles deposited in the olfactory region, and by increasing to 8.1×10^7 A/m, about 45% deposit in the olfactory region. A recommended magnet layout, including the magnet strength as well as the resultant particle trajectories, is shown in **Figure 7A**.

The predicted olfactory dosage in the 3-D nose model with the recommended magnet layout is shown in **Figure 7B**. Similar to the 2-D case, magnetophoretic guidance significantly improves olfactory dosages, and that point-release is superior to the conventional release from the entire nostril. With appropriate magnetophoretic guidance, the delivered olfactory dose can be one or even two orders of magnitude higher compared to that without magnetophoretic guidance (45% in **Figure 7B** vs. < 0.1% in **Figure 3**). **Figure 7B** also shows the variation of the 3-D olfactory dosage as a function of carrier droplet size. There is negligible olfactory deposition for $d'_p < 10$ μm or $d'_p > 20$ μm; the former is due to weak magnetic responsiveness, while the latter is due to the high inertia loss to the anterior nose. The optimal olfactory deposition comes from aerosols in the range of 13 − 17 μm, with a median size of 15 μm.

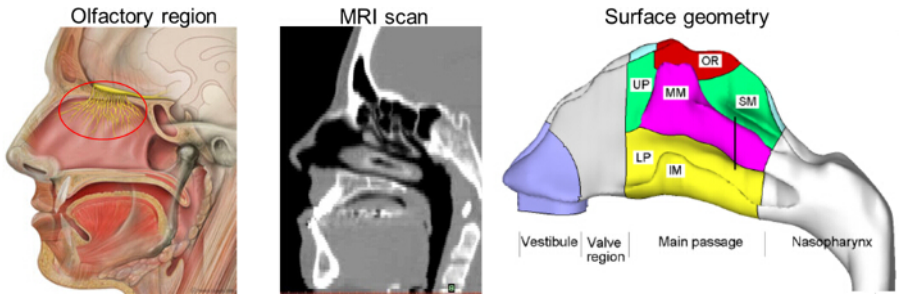

Figure 1. Human Nose Model and the Olfactory Region that is Located at the very top of the Nasal Cavity. The complex structure of the nose prevents effective drug delivery to the olfactory region with standard nasal devices. To study deposition distributions, the MRI-based nose model was divided into different sections. LP: lower passage, UP: upper passage, MM: middle meatus, SM: superior meatus, OR: olfactory region. Please click here to view a larger version of this figure.

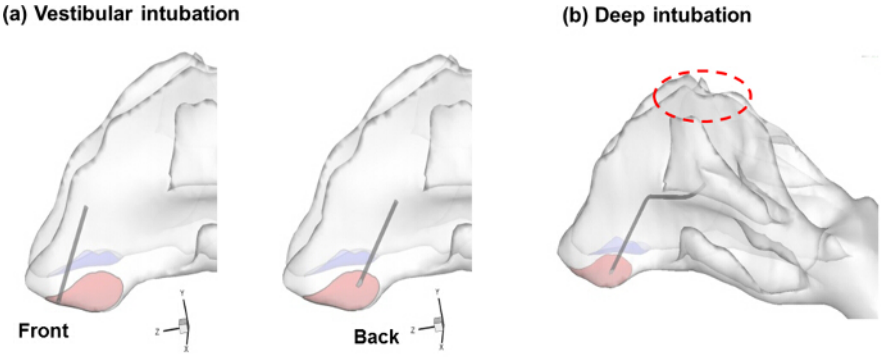

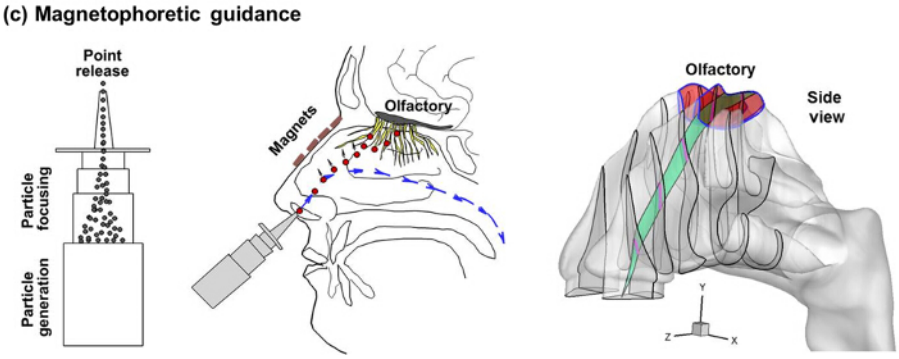

Figure 2. Three Olfactory Delivery Protocols. (A) vestibular intubation **(B)** deep intubation, and **(C)** magnetophoretic guidance of ferromagnetic particles. For optimal olfactory drug delivery, particles should travel along the middle plane of the nasal passage. Please click here to view a larger version of this figure.

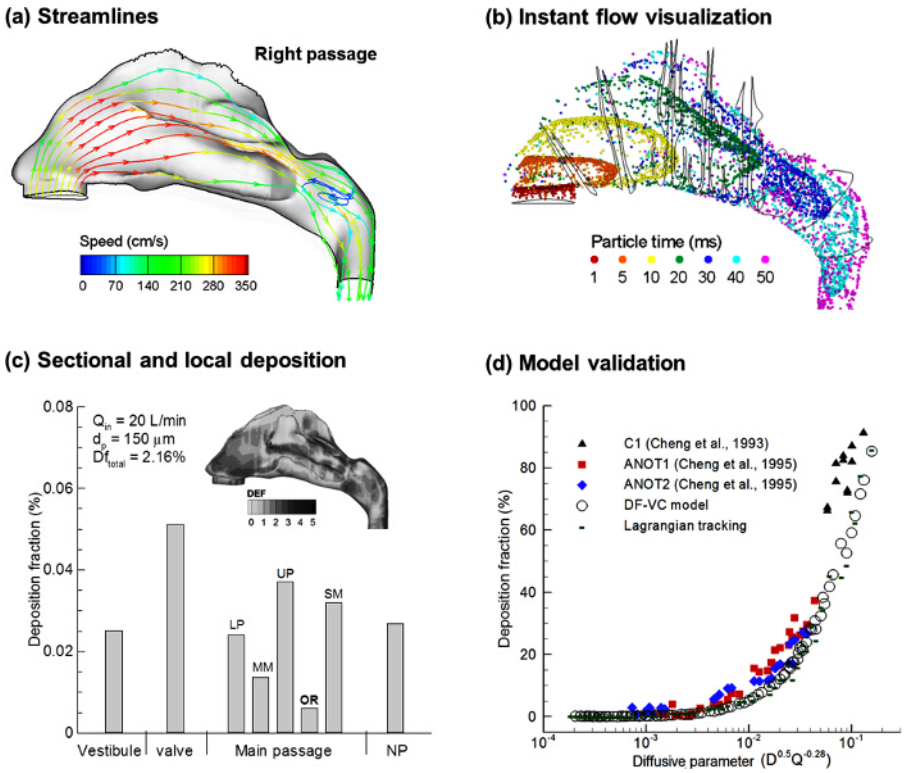

Figure 3. Control Case. (A) airflow streamlines and **(B)** snapshots of particle motion at varying instants. **(C)** Deposition pattern is highly heterogeneous, with high particle accumulations in the anterior nose; **(D)** good agreement is achieved between the numerically predicted and experimental measurements. NP: nasopharynx. Please click here to view a larger version of this figure.

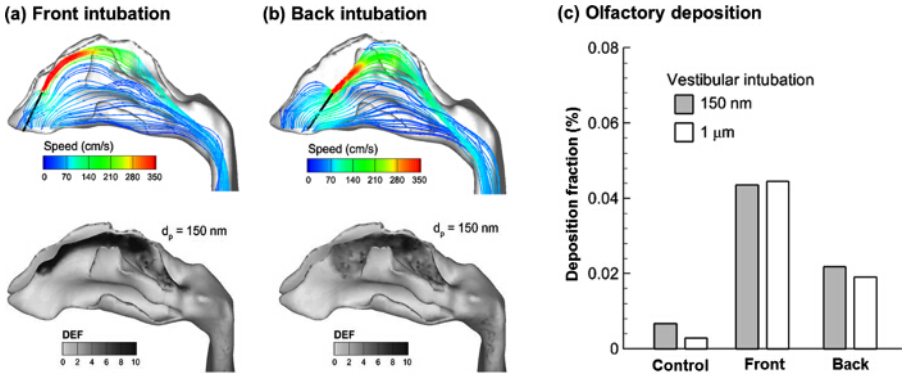

Figure 4. Airflow Streamlines and Particle Depositions in the Vestibular Intubation Protocol. (A) front intubation **(B)** back intubation. Comparison of the olfactory doses is shown in **(C)** for 150 nm and 1 μm particles. Please click here to view a larger version of this figure.

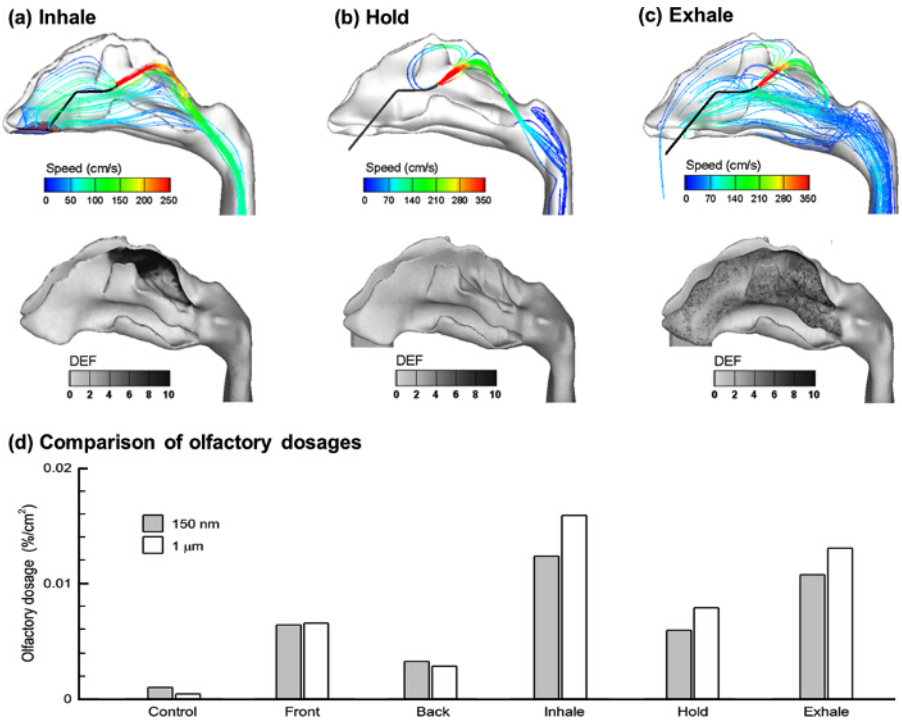

Figure 5. Airflow Streamlines and Particle Deposition with Deep Intubation under Three Breathing Conditions. (A) inhalation **(B)** breath-holding, and **(C)** exhalation. Comparison of the normalized olfactory doses (mass fraction per cm^2) among different protocols is shown in **(D)**. Please click here to view a larger version of this figure.

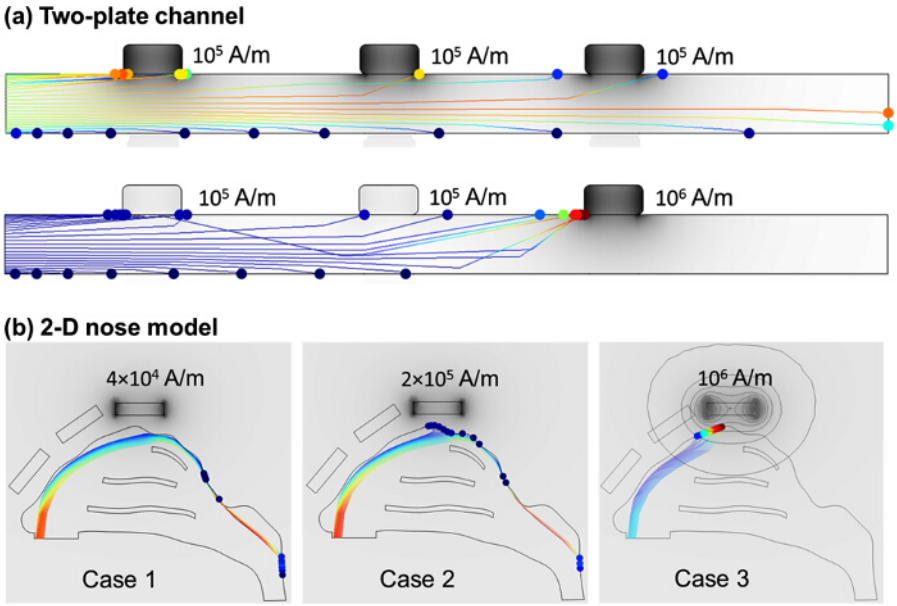

Figure 6. Magnetic Field and Particle Trajectories in (A) a two-plate channel and **(B)** an idealized 2-D nose model. A darker color in the proximity of the magnets represents a stronger magnetic field. Please click here to view a larger version of this figure.

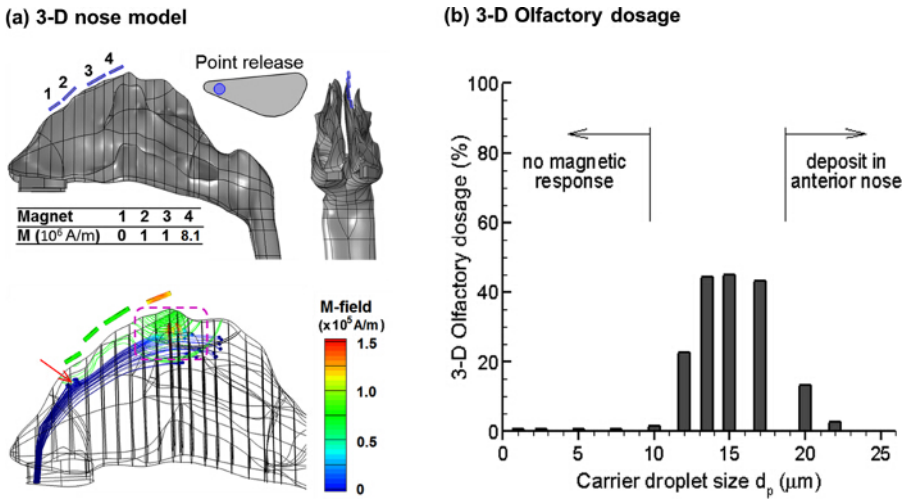

Figure 7. Magnetophoretc Guidance in a 3-D Nose Model: (A) magnet layout and particle trajectories, and **(B)** variation of the olfactory dosages as a function of particle size. Please click here to view a larger version of this figure.

Discussion

A coupled image-CFD method was presented in this study that incorporated the image-based model development, quality meshing, airflow simulation, and magnetic particle tracking. Multiple software modules were implemented to this aim, which included functions of segmentation of medical images, reconstruction/meshing of anatomically accurate airway models, and flow-particle simulations. Using this numerical method, performances of three intranasal delivery protocols were tested and compared. Compared to *in vitro* experiments, this method is more efficient in cost and time; thus a large number of numerical tests can be conducted to identify the optimal delivery protocol[25,26]. In particular, the coupled image-CFD method generates detailed information on the behavior and fates of drug particles, thereby providing in-depth insights in reducing drug loss in the anterior nose and increasing drug dosages to the target. Furthermore, the coupled image-CFD method developed in this study can be easily modified for intranasal drug delivery to other regions such as paranasal sinuses[24]. Similar procedures can be followed as outlined in the protocol except the following two procedures. (1) The region of interest that was predefined in 2.1.3 should be changed to the sinus, which can be achieved by following the protocol 1.4. (2) The range of magnet configuration and strength need to be adjusted for sinus drug delivery. The path of a drug particle from the nostril to the sinus is dramatically different from that from the nostril to the olfactory. The magnetic field should be accordingly modified so that the particles can be guided to follow predefined paths. This task can be achieved by following protocol 3.2.1.

There are two critical steps in modeling the olfactory drug delivery with this image-CFD method. First, developing an image-based nose model that is acceptable to flow-particle-simulation software (*e.g.*, Fluent and COMSOL) still remains a challenge. It took more than 60 hr to reconstruct the surface geometry of the current nose model (Protocol 1.3). Second, simulation results show that magnetic particles are very sensitive to magnetic field and particle release position; extensive testing of magnet layout is required before reaching the optimal delivery design (Protocol 3.2.3 and 3.3.2).

All three drug delivery protocols were predicted to give improved olfactory doses; however, the improvement differed among the three methods. The two passive-control protocols (vestibular and deep intubation) appear inadequate to attain sufficient CNS doses without causing significant drug losses to other regions in the nose. Even for the optimal passive-control protocol (*i.e.*, deep intubation under inhalation conditions), the olfactory dosage is still too low (< 0.1%) to be practical for the purpose of direct nose-to-brain delivery. Active controls of drug particles in the nasal cavity are indispensable. Limitations of this study include the assumption of steady flows, rigid airway walls, numerical modeling only, and the use of one nasal airway geometry. Therefore, results of this study cannot account for intersubjective variability. For drug delivery to a different person, the design proposed herein is expected to have lower performance. To achieve the optimal delivery to that specific patient, a personalized design should be formulated based on the patient's nasal geometry.

The proposed olfactory delivery protocol has important implications in direct nose-to-brain drug delivery. Standard nasal devices deliver extremely low doses (< 1%) to the olfactory region, which has forestalled the use of many new genetically engineered drugs for treating CNS disorders such as Alzheimer's disease and brain tumors[1,9]. The proposed magnetophoretic olfactory delivery is promising to deliver clinically significant dosage to the olfactory region and provides a noninvasive practical method of bypassing the blood-brain barrier. This delivery system can also be readily adapted for delivering drugs to other regions in the nose such as paranasal sinuses, in a different nose model, or for drugs with different physical properties.

Disclosures

The authors report no conflicts of interest in this work.

Acknowledgements

This study was funded by Central Michigan University Innovative Research Grant P421071 and Early Career Grant P622911.

References

1. Mistry, A., Stolnik, S., Illum, L. Nanoparticles for direct nose-to-brain delivery of drugs. *Int. J. Pharm.* **379**(1), 146-157 (2009).
2. Alam, S. *et al.* Development and evaluation of thymoquinone-encapsulated chitosan nanoparticles for nose-to-brain targeting: a pharmacoscintigraphic study. *Int. J. Nanomedicine.* **7**(11), 5705-5718 (2012).
3. Shi, H., Kleinstreuer, C., Zhang, Z. Laminar airflow and nanoparticle or vapor deposition in a human nasal cavity model. *J. Biomech. Eng.* **128**(5), 697-706 (2006).
4. Si, X., Xi, J., Kim, J., Zhou, Y., Zhong, H. Modeling of release position and ventilation effects on olfactory aerosol drug delivery. *Respir. Physiol. Neurobiol.* **186**(1), 22-32 (2013).
5. Si, X., Xi, J., Kim, J. Effect of laryngopharyngeal anatomy on expiratory airflow and submicrometer particle deposition in human extrathoracic airways. *Open J. Fluid D.* **3**(4), 286-301 (2013).
6. Xi, J., Longest, P.W. Numerical predictions of submicrometer aerosol deposition in the nasal cavity using a novel drift flux approach. *Int. J. Heat Mass Transfer.* **51**(23), 5562-5577 (2008).
7. Illum, L. Nasal drug delivery: new developments and strategies. *Drug Discov. Today.* **7**(23), 1184-1189 (2002).
8. El Taoum, K.K., Xi, J., Kim, J.W., Berlinski, A. *In vitro* evaluation of aerosols delivered via the nasal route. *Respir. Care.* **60**(7), 1015-1025 (2015).
9. Misra, A., Kher, G. Drug delivery systems from nose to brain. *Curr. Pharm. Biotechnol.* **13**(12), 2355-2379 (2012).
10. Hoekman, J.D., Ho, R.J.Y. Effects of Localized Hydrophilic Mannitol and Hydrophobic Nelfinavir Administration Targeted to Olfactory Epithelium on Brain Distribution. *Aaps Pharmscitech.* **12**(2), 534-543 (2011).
11. Corley, R.A. *et al.* Comparative Computational Modeling of Airflows and Vapor Dosimetry in the Respiratory Tracts of Rat, Monkey, and Human. *Toxicol. Sci.* **128**(2), 500-516 (2012).
12. Shi, H., Kleinstreuer, C., Zhang, Z. Modeling of inertial particle transport and deposition in human nasal cavities with wall roughness. *J. Aerosol Sci.* **38**(4), 398-419 (2007).
13. Kleinstreuer, C., Zhang, Z., Donohue, J.F. Targeted drug-aerosol delivery in human respiratory system. *Annu. Rev. Biomed. Eng.* **10**(4), 195-220 (2008).
14. Kleinstreuer, C., Zhang, Z., Li, Z., Roberts, W.L., Rojas, C. A new methodology for targeting drug-aerosols in the human respiratory system. *Int. J. Heat Mass Transfer.* **51**(23), 5578-5589 (2008).
15. Wilson, I.B. The deposition of charged particles in tubes, with reference to the retention of therapeutic aerosols in the human lung. *J. Colloid Sci.* **2**(2), 271-276 (1947).
16. Wong, J., Chan, H.-K., Kwok, P.C.L. Electrostatics in pharmaceutical aerosols for inhalation. *Ther Deliv.* **4**(8), 981-1002 (2013).
17. Bailey, A.G. The inhalation and deposition of charged particles within the human lung. *Journal of Electrostatics.* **42**(1), 25-32 (1997).
18. Xi, J., Si, X.A., Gaide, R. Electrophoretic particle guidance significantly enhances olfactory drug delivery: a feasibility study. *PLoS ONE.* **9**(1), e86593 (2014).
19. Martin, A., Finlay, W. Alignment of magnetite-loaded high aspect ratio aerosol drug particles with magnetic fields. *Aerosol Sci. Technol.* **42**(4), 295-298 (2008).
20. Dames, P. *et al.* Targeted delivery of magnetic aerosol droplets to the lung. *Nature Nanotechnology.* **2**(8), 495-499 (2007).
21. Xi, J., Longest, P.W. Transport and deposition of micro-aerosols in realistic and simplified models of the oral airway. *Ann. Biomed. Eng.* **35**(4), 560-581 (2007).
22. Longest, P.W., Xi, J. Effectiveness of direct Lagrangian tracking models for simulating nanoparticle deposition in the upper airways. *Aerosol Sci. Technol.* **41**(4), 380-397 (2007).
23. Xi, J., Zhang, Z., Si, X.A., Yang, J., Deng, W. Optimization of magnetophoretic-guided drug delivery to the olfactory region in a human nose model. *Biomech. Model. Mechanobiol.* **In press**(Sept), 1-15 (2015).
24. Longest, P.W., Hindle, M., Das Choudhuri, S., Xi, J.X. Comparison of ambient and spray aerosol deposition in a standard induction port and more realistic mouth-throat geometry. *J. Aerosol Sci.* **39**(7), 572-591 (2008).
25. Xi, J. *et al.* Design and Testing of Electric-Guided Delivery of Charged Particles to the Olfactory Region: Experimental and Numerical Studies. *Curr. Drug Deliv.* **13**(9), 1-15 26362143 (2015).
26. Zhou, Y., Guo, M., Xi, J., Irshad, H., Cheng, Y.-S. Nasal deposition in infants and children. *Journal of aerosol medicine and pulmonary drug delivery.* **27**(2), 110-116 (2014).
27. Xi, J., Yuan, J.E., Si, X.A., Hasbany, J. Numerical optimization of targeted delivery of charged nanoparticles to the ostiomeatal complex for treatment of rhinosinusitis. *Int. J. Nanomedicine.* **10**(7), 4847-4861 (2015).

